Journal of Sound and Vibration (1997) **204**(4), 645–657

VIBRATION ANALYSIS OF STEPPED THICKNESS PLATES

S. J. Guo

Department of Mechanical Engineering, University of Humberside, Cottingham Road, Hull, HU6 7RT, England

AND

A. J. Keane and M. Moshrefi-Torbati

Department of Mechanical Engineering, University of Southampton, Highfield, Southampton, SO17 1BJ, England

(*Received* 26 *April* 1996, *and in final form* 11 *February* 1997)

Investigation has been made into various approaches for analyzing the vibration of plates with stepped thicknesses. First, attention has been paid to updating a classical approach for the analysis of such problems, correcting the boundary conditions cited in an earlier paper and dealing with the difficulties that can arise when calculating high order modes. Secondly, contribution has been made to improving the classical finite strip method (FSM) by replacing the "static" shape function of the strip element model by a "dynamic" function. This leads to the development of a dynamic finite strip method which improves solution accuracy without compromising model size and which therefore is more efficient than the classical FSM. When compared with the finite element method (FEM), which is also considered here, the advantages of smaller model size and higher accuracy of the dynamic FSM are significant. In order to demonstrate the application of the above approaches, the modes of simply supported plates with uniform and stepped thicknesses have been analyzed. From this numerical study, it is noted that the updated classical approach can be used to obtain a solution for any order mode to any specified accuracy and is the most efficient approach considered in the present study. It is also noted that, compared with the FEM of similar solution accuracy, the dynamic finite strip method normally produces a much smaller model size, so that such calculations are significantly more efficient than for the FEM. The aim of this work is to establish efficient methods for the analysis of stepped plates that might be used in optimization studies where speed of formulation and solution are at a premium. There are, of course, a number of other methods that could be used to tackle such problems, but they lie outside the scope of this work; see for example the papers of Liew and co-authors [1, 2].

1. INTRODUCTION

The main purpose of this work is to obtain efficient methods for the structural dynamic analysis of stepped thickness plates when accurate high order modes are required. As is well known when carrying out modal analysis using a discrete numerical approach, such as the finite element method (FEM) or finite strip method (FSM), the number of modes that may be solved and the solution accuracy of these modes, depends to a great extent upon the meshing or element size. This somewhat limits application of the FEM, especially when both high order modes and optimization are involved. On the other hand, application of analytical approaches is usually limited to very simple cases such as a

0022–460X/97/290645 + 13 $25.00/0/sv970955

vibrating plate with simply supported boundary conditions where exact solutions can be obtained. In the current work, attention has been paid to improving the classical FSM, since this method has some features in favour of the application case of interest here.

The finite strip method (FSM) presented by Cheung [3] has been developed and applied to various structural dynamic analyses successfully. The main advantage of the method is its efficiency and accuracy, especially for structures with regular geometry. This is because it combines the versatility of the finite element method (FEM) with the rapid convergence of the Ritz approach, by selecting proper trial functions *a priori*. Compared to the FEM, the model size used by the FSM is usually smaller, since unlike the FEM, in which meshing normally needs to be implemented in all dimensions, the FSM uses modal functions instead of polynomials and meshing in at least one dimension for a multi-dimensional problem. To take plate bending vibration as an example, strip element (beam) vibration modal functions are normally used as part of the plate displacement function, without discretization in the longitudinal direction and polynomials (namely the shape functions) are used to represent deformation of the strip elements. This feature is of significant advantage, especially when high order modes are required, since the dependency of the accuracy upon the model size is then reduced to a large extent. However, the structural model still has to be discretized in at least one dimension. This provides flexibility in the element model assembly and application, but the disadvantage of solution dependency upon the meshing or model size remains.

In order to improve the classical FSM, attention has been paid to the improvement of the shape functions. In theory, the shape function should be replaced by the displacement function from the differential equation of a vibrating beam. However, this results in a frequency dependent stiffness matrix which causes some difficulties. In order to maintain the efficiency of the FSM, the frequency dependent displacement function of the strip in its transverse direction is represented as a series in terms of increasing powers of frequency. This approach has been applied to the development of the so called dynamic finite element method [4, 5, 6]. In this manner, the frequency can be removed from the displacement function which makes the eigen-problem easier to solve. In addition, the number of terms in the series included in the strip model can be chosen by the user, which reduces the dependency of the model accuracy upon the strip element size in the transverse direction, although meshing is not totally removed. In addition, based as it is on a displacement approach, the strip element model in the FSM must be C1-continuous to make the FSM applicable to the vibration of a plate with abrupt change of thickness, which is the case being dealt with here. It is noted that a new finite strip method has been developed by Cheung and Kong [7] and applied to the vibration of plates with stepped thickness. However, unlike the dynamic FSM, to refine the displacement function, the modal functions of the classical method are simplified in Cheung's new method by using static modes while the shape functions remain cubic Hermitian functions.

In order to demonstrate the application and efficiency of the dynamic finite strip method, simply supported thin plates with uniform thickness and abrupt thickness changes are taken as examples and the classical and dynamic FSM are used. To assess the accuracy of these methods, the classical approach developed by Chopra [8] for the vibration of a plate with thickness change has also been applied to these cases. However, it is noted that when applying this approach for high order modes, the matrix, on which the eigenvalue calculations are based, can become ill-conditioned and then difficulty arises in obtaining zero determinants. Therefore, attention has also been paid to overcoming this difficulty in the current work. It is also noted that in the original paper by Chopra [8] an

inappropriate set of boundary conditions was adopted and these have been revised here.

The modal results from these various methods are compared and discussed in what follows. For the two examples considered, it is known that the FE models have much larger sizes than the FS models and are therefore less efficient. When the FS model is further reduced as shown in Example 2, although the solution accuracy from the classical FSM is affected, it can be improved by applying the dynamic FSM which is seen to be the more efficient approach in this case.

2. CLASSICAL METHOD

A classical method for the vibration of a stepped thickness plate based on the work of Chopra [8] has been developed and initially applied to a plate with one change in thickness. In order to deal with the vibration problem of a multi-stepped thickness plate as shown in Figure 1, especially for high order modes, further investigation into the practical use and extension of the method has been carried out. Theoretically, by dividing the whole plate into parts according to its thickness changes in the longitudinal direction, each part of the plate is then of uniform thickness and can be represented by the following governing differential equation under the assumption of sinusoidal movement for free vibration:

$$(\nabla^4 - k_i^4)W_i = 0 \qquad x_i \leqslant x \leqslant x_{i+1} \qquad i = 1, 2, \ldots, J+1. \tag{1}$$

Here the subscript i represents the ith part of a plate of $J+1$ sections and $k_i^4 = \rho\omega^2 t_i/D_i$; W_i is the displacement function of the ith part for which the general solution is

$$W_i(\xi, \eta) = \sum_n S_{in}(\xi) \sin(n\pi\eta), \tag{2}$$

with the shape function

$$S_{in}(\xi) = A_{in} \sin(\lambda_{i1}\xi) + B_{in} \cos(\lambda_{i1}\xi) + C_{in} \sinh(\lambda_{i2}\xi) + D_{in}\cosh(\lambda_{i2}\xi), \tag{3}$$

where $\lambda_{i1} = a\sqrt{k_i^2 - \alpha^2}$, $\lambda_{i2} = a\sqrt{k_i^2 + \alpha^2}$ and A_{in}, B_{in}, C_{in} and D_{in} are unknown coefficients. (A list of notation is given in the Appendix.)

First, by introducing the boundary conditions, such as the simply supported edges in the current case, the shape function for the first and last parts of the plate can be simplified with fewer unknown coefficients as follows:

$$S_{1n}(\xi) = A_{1n} \sin \lambda_{11}\xi + C_{1n} \sinh \lambda_{12}\xi, \tag{4a}$$

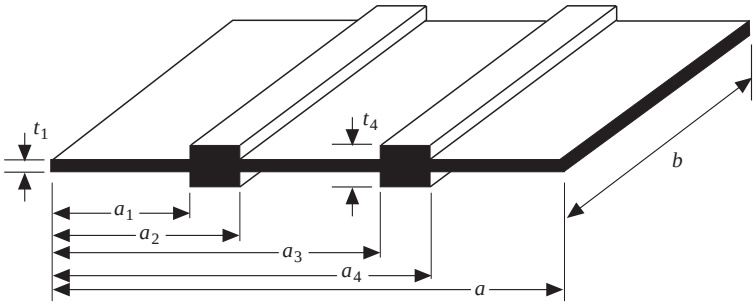

Figure 1. A simply supported plate with two stiffeners.

$$S_{J+1,n}(\xi) = A_{J+1,n}(\sin \lambda_{J+1,1}\xi - \tan \lambda_{J+1,1} \cos \lambda_{J+1,1}\xi)$$

$$+ C_{J+1,n}(\sinh \lambda_{J+1,2}\xi - \tanh \lambda_{J+1,2} \cosh \lambda_{J+1,2}\xi). \quad (4b)$$

Secondly, by substituting equations (2) and (4) into the following continuity conditions which should be satisfied along each of the joint lines located at ξ_i,

$$\left.\begin{aligned} W_i(\xi, \eta) &= W_{i+1}(\xi, \eta) \\ W_i'(\xi, \eta) &= W_{i+1}'(\xi, \eta) \\ D_i\left\{\frac{\partial^2 W_i(\xi, \eta)}{\partial x^2} + v\frac{\partial^2 W_i(\xi, \eta)}{\partial y^2}\right\} &= D_{i+1}\left\{\frac{\partial^2 W_{i+1}(\xi, \eta)}{\partial x^2} + v\frac{\partial^2 W_{i+1}(\xi, \eta)}{\partial y^2}\right\} \\ D_i\left\{\frac{\partial^3 W_i(\xi, \eta)}{\partial x^3} + (2-v)\frac{\partial^3 W_i(\xi, \eta)}{\partial x \partial y^2}\right\} &= D_{i+1}\left\{\frac{\partial^3 W_{i+1}(\xi, \eta)}{\partial x^3} + (2-v)\frac{\partial^3 W_{i+1}(\xi, \eta)}{\partial x \partial y^2}\right\} \end{aligned}\right\} \text{ at } \xi = \xi_i, \quad (5)$$

four equations corresponding to each joint line can be established. (It should be noted that in the original work by Chopra [8] the last two of these conditions are incorrectly specified as $W_i''(\xi, \eta) = W_{i+1}''(\xi, \eta)$ and $W_i'''(\xi, \eta) = W_{i+1}'''(\xi, \eta)$ which, of course, hold only when there is no change in plate properties across the joint.)

For a plate with two different thickness parts joined along the line at ξ_1, the four equations can be written in matrix form as

$$\begin{bmatrix} \sin \lambda_{11}\xi_1 & \sinh \lambda_{12}\xi_1 \\ \lambda_{11} \cos \lambda_{11}\xi_1 & \lambda_{12} \cosh \lambda_{12}\xi_1 \\ -D_1\{\lambda_{11}^2 + v\alpha^2\} \sin \lambda_{11}\xi_1 & D_1\{\lambda_{12}^2 - v\alpha^2\} \sinh \lambda_{12}\xi_1 \\ -D_1\lambda_{11}\{\lambda_{11}^2 + (2-v)\alpha^2\} \cos \lambda_{11}\xi_1 & D_1\lambda_{12}\{\lambda_{12}^2 - (2-v)\alpha^2\} \cosh \lambda_{12}\xi_1 \end{bmatrix}$$

$$\begin{bmatrix} -(\sin \lambda_{21}\xi_1 - \tan \lambda_{21} \cos \lambda_{21}\xi_1) & -(\sinh \lambda_{22}\xi_1 - \tanh \lambda_{22} \cosh \lambda_{22}\xi_1) \\ -\lambda_{21}(\cos \lambda_{21}\xi_1 + \tan \lambda_{21} \sin \lambda_{21}\xi_1) & -\lambda_{22}(\cosh \lambda_{22}\xi_1 - \tanh \lambda_{22} \sinh \lambda_{22}\xi_1) \\ D_2\{\lambda_{21}^2 + v\alpha^2\} (\sin \lambda_{21}\xi_1 - \tan \lambda_{21} \cos \lambda_{21}\xi_1) & \\ & -D_2\{\lambda_{22}^2 - v\alpha^2\} (\sinh \lambda_{22}\xi_1 - \tanh \lambda_{22} \cosh \lambda_{22}\xi_1) \\ D_2\lambda_{21}\{\lambda_{21}^2 + (2-v)\alpha^2\}(\cos \lambda_{21}\xi_1 + \tan \lambda_{21} \sin \lambda_{21}\xi_1) & \\ & -D_2\lambda_{22}\{\lambda_{22}^2 - (2-v)\alpha^2\} (\cosh \lambda_{22}\xi_1 - \tanh \lambda_{22} \sinh \lambda_{22}\xi_1) \end{bmatrix}$$

$$\times \begin{Bmatrix} A_{1n} \\ C_{1n} \\ A_{2n} \\ C_{2n} \end{Bmatrix} = \{0\}. \quad (6)$$

The eigenvalues of the vibrating plate can be obtained from the ω included in the λ of the above equations which make the determinant of the above 4×4 coefficient matrix zero. Relative values of the coefficients A_{1n}, C_{1n}, A_{2n} and C_{2n} corresponding to any eigenvalue can then be calculated by solving a reduced inhomogeneous equation and substituting back into equations (4) and (2) to obtain the corresponding mode shapes.

For the general case of a plate with multi-thickness parts joined at J joint lines, the continuity conditions in equation (5) have to be applied to equation (2) at each joint line. This results in $4 \times J$ equations: at joint 1,

$$A_{1n}\sin\lambda_{11}\xi_1 + C_{1n}\sinh\lambda_{12}\xi_1 - A_{2n}\sin\lambda_{21}\xi_1 - B_{2n}\cos\lambda_{21}\xi_1 - C_{2n}\sinh\lambda_{22}\xi_1 - D_{2n}\cosh\lambda_{22}\xi_1 = 0,$$

$$A_{1n}\lambda_{11}\cos\lambda_{11}\xi_1 + C_{1n}\lambda_{12}\cosh\lambda_{12}\xi_1 - A_{2n}\lambda_{21}\cos\lambda_{21}\xi_1 + B_{2n}\lambda_{21}\sin\lambda_{21}\xi_1$$
$$- C_{2n}\lambda_{22}\cosh\lambda_{22}\xi_1 - D_{2n}\lambda_{22}\sinh\lambda_{22}\xi_1 = 0,$$

$$- A_{1n}D_1\{\lambda_{11}^2 + \nu\alpha^2\}\sin\lambda_{11}\xi_1 + C_{1n}D_1\{\lambda_{12}^2 - \nu\alpha^2\}\sinh\lambda_{12}\xi_1$$
$$+ A_{2n}D_2\{\lambda_{21}^2 + \nu\alpha^2\}\sin\lambda_{21}\xi_1 + B_{2n}D_2\{\lambda_{21}^2 + \nu\alpha^2\}\cos\lambda_{21}\xi_1$$
$$- C_{2n}D_2\{\lambda_{22}^2 - \nu\alpha^2\}\sinh\lambda_{22}\xi_1 - D_{2n}D_2\{\lambda_{22}^2 - \nu\alpha^2\}\cosh\lambda_{22}\xi_1 = 0,$$

$$- A_{1n}D_1\lambda_{11}\{\lambda_{11}^2 + (2-\nu)\alpha^2\}\cos\lambda_{11}\xi_1 + C_{1n}D_1\lambda_{12}\{\lambda_{12}^2 - (2-\nu)\alpha^2\}\cosh\lambda_{12}\xi_1$$
$$+ A_{2n}D_2\lambda_{21}\{\lambda_{21}^2 + (2-\nu)\alpha^2\}\cos\lambda_{21}\xi_1 - B_{2n}D_2\lambda_{21}\{\lambda_{21}^2 + (2-\nu)\alpha^2\}\sin\lambda_{21}\xi_1$$
$$- C_{2n}D_2\lambda_{22}\{\lambda_{22}^2 - (2-\nu)\alpha^2\}\cosh\lambda_{22}\xi_1$$
$$- D_{2n}D_2\lambda_{22}\{\lambda_{22}^2 - (2-\nu)\alpha^2\}\sinh\lambda_{22}\xi_1 = 0; \tag{7a}$$

at joints $j = 2, \ldots, (J-1)$,

$$A_{jn}\sin\lambda_{j1}\xi_j + B_{jn}\cos\lambda_{j1}\xi_j + C_{jn}\sinh\lambda_{j2}\xi_j + D_{jn}\cosh\lambda_{j2}\xi_j$$
$$- A_{j+1,n}\sin\lambda_{j+1,1}\xi_j - B_{j+1,n}\cos\lambda_{j+1,1}\xi_j - C_{j+1,n}\sinh\lambda_{j+1,2}\xi_j$$
$$- D_{j+1,n}\cosh\lambda_{j+1,2}\xi_j = 0,$$

$$A_{jn}\cos\lambda_{j1}\xi_j - B_{jn}\lambda_{j1}\sin\lambda_{j1}\xi_j + C_{jn}\lambda_{j2}\cosh\lambda_{j2}\xi_j + D_{jn}\lambda_{j2}\sinh\lambda_{j2}\xi_j$$
$$- A_{j+1,n}\lambda_{j+1,1}\cos\lambda_{j+1,1}\xi_j + B_{j+1,n}\lambda_{j+1,1}\sin\lambda_{j+1,1}\xi_j$$
$$- C_{j+1,n}\lambda_{j+1,2}\cosh\lambda_{j+1,2}\xi_j - D_{j+1,n}\lambda_{j+1,2}\sinh\lambda_{j+1,2}\xi_j = 0,$$

$$- A_{jn}D_j\{\lambda_{j1}^2 + \nu\alpha^2\}\sin\lambda_{j1}\xi_j - B_{jn}D_j\{\lambda_{j1}^2 + \nu\alpha^2\}\cos\lambda_{j1}\xi_j + C_{jn}D_j\{\lambda_{j2}^2 - \nu\alpha^2\}\sinh\lambda_{j2}\xi_j$$
$$+ D_{jn}D_j\{\lambda_{j2}^2 - \nu\alpha^2\}\cosh\lambda_{j2}\xi_j$$
$$+ A_{j+1,n}D_{j+1}\{\lambda_{j+1,1}^2 + \nu\alpha^2\}\sin\lambda_{j+1,1}\xi_j + B_{j+1,n}D_{j+1}\{\lambda_{j+1,1}^2 + \nu\alpha^2\}\cos\lambda_{j+1,1}\xi_j$$
$$- C_{j+1,n}D_{j+1}\{\lambda_{j+1,2}^2 - \nu\alpha^2\}\sinh\lambda_{j+1,2}\xi_j$$
$$- D_{j+1,n}D_{j+1}\{\lambda_{j+1,2}^2 - \nu\alpha^2\}\cosh\lambda_{j+1,2}\xi_j = 0,$$

$$- A_{jn}D_j\lambda_{j1}\{\lambda_{j1}^2 + (2-\nu)\alpha^2\}\cos\lambda_{j1}\xi_j + B_{jn}\{\lambda_{j1}^2 + (2-\nu)\alpha^2\}\sin\lambda_{j1}\xi_j$$
$$+ C_{jn}D_j\lambda_{j2}\{\lambda_{j2}^2 - (2-\nu)\alpha^2\}\cosh\lambda_{j2}\xi_j + D_{jn}D_j\lambda_{j2}\{\lambda_{j2}^2 - (2-\nu)\alpha^2\}\sinh\lambda_{j2}\xi_j$$
$$+ A_{j+1,n}D_{j+1}\lambda_{j+1,1}\{\lambda_{j+1,1}^2 + (2-\nu)\alpha^2\}\cos\lambda_{j+1,1}\xi_j$$
$$- B_{j+1,n}D_{j+1}\lambda_{j+1,1}\{\lambda_{j+1,1}^2 + (2-\nu)\alpha^2\}\sin\lambda_{j+1,1}\xi_j$$
$$- C_{j+1,n}D_{j+1}\lambda_{j+1,2}\{\lambda_{j+1,2}^2 - (2-\nu)\alpha^2\}\cosh\lambda_{j+1,2}\xi_j$$
$$- D_{j+1,n}D_{j+1}\lambda_{j+1,2}\{\lambda_{j+1,2}^2 - (2-\nu)\alpha^2\}\sinh\lambda_{j+1,2}\xi_j = 0; \tag{7b}$$

and at the last joint J,

$$A_{Jn}\sin\lambda_{J1}\xi_J + B_{Jn}\cos\lambda_{J1}\xi_J + C_{Jn}\sinh\lambda_{J2}\xi_J + D_{Jn}\cosh\lambda_{J2}\xi_J$$
$$- A_{j+1,n}(\sin\lambda_{J+1,1}\xi_J - \tan\lambda_{J+1,1}\cos\lambda_{J+1,1}\xi_J)$$

$$
\begin{aligned}
&- C_{J+1,n}(\sinh \lambda_{J+1,2}\xi_J - \tanh \lambda_{J+1,2} \cosh \lambda_{J+1,2}\xi_J) = 0,\\
&A_{Jn}\lambda_{J1} \cos \lambda_{J1}\xi_J - B_{Jn}\lambda_{J1} \sin \lambda_{J1}\xi_J + C_{Jn}\lambda_{J2} \cosh \lambda_{J2}\xi_J + D_{Jn}\lambda_{J2} \sinh \lambda_{J2}\xi_J\\
&- A_{J+1,n}\lambda_{J+1,1}(\cos \lambda_{J+1,1}\xi_j + \tan \lambda_{J+1,1} \sin \lambda_{J+1,1}\xi_J)\\
&- C_{J+1,n}\lambda_{J+1,2}(\cosh \lambda_{J+1,2}\xi_J - \tanh \lambda_{J+1,2} \sinh \lambda_{J+1,2}\xi_J) = 0,\\
&\quad - A_{Jn}D_J\{\lambda_{J1}^2 + v\alpha^2\} \sin \lambda_{J1}\xi_J - B_{Jn}D_J\{\lambda_{J1}^2 + v\alpha^2\} \cos \lambda_{J1}\xi_j\\
&\quad + C_{Jn}D_J\{\lambda_{J2}^2 - v\alpha^2\} \sinh \lambda_{J2}\xi_J + D_{Jn}D_J\{\lambda_{J2}^2 - v\alpha^2\} \cosh \lambda_{J2}\xi_J\\
&\quad - A_{J+1,n}D_{J+1}\{\lambda_{J+1,1}^2 + v\alpha^2\}(\sin \lambda_{J+1,1}\xi_J - \tan \lambda_{J+1,1} \cos \lambda_{J+1,1}\xi_J)\\
&\quad - C_{J+1,n}D_{J+1}\{\lambda_{J+1,2}^2 - v\alpha^2\}(\sinh \lambda_{J+1,2}\xi_J\\
&\quad - \tanh \lambda_{J+1,2} \cosh \lambda_{J+1,2}\xi_J) = 0,\\
&- A_{Jn}D_J\lambda_{J1}\{\lambda_{J1}^2 + (2-v)\alpha^2\} \cos \lambda_{J1}\xi_J + B_{Jn}D_J\lambda_{J1}\{\lambda_{J1}^2 + (2-v)\alpha^2\} \sin \lambda_{J1}\xi_J\\
&+ C_{Jn}D_J\lambda_{J2}\{\lambda_{J2}^2 - (2-v)\alpha^2\} \cosh \lambda_{J2}\xi_J + D_{Jn}D_J\lambda_{J2}\{\lambda_{J2}^2 - (2-v)\alpha^2\} \sinh \lambda_{J2}\xi_J\\
&+ A_{J+1,n}D_{J+1}\lambda_{J+1,1}\{\lambda_{J+1,1}^2 + (2-v)\alpha^2\} \cos \lambda_{J+1,1}\xi_J + \tan \lambda_{J+1,1} \sin \lambda_{J+1,1}\xi_J)\\
&- C_{J+1,n}D_{J+1}\lambda_{J+1,2}\{\lambda_{J+1,2}^2 - (2-v)\alpha^2\}(\cosh \lambda_{J+1,2}\xi_J\\
&- \tan \lambda_{J+1,2} \sinh \lambda_{J+1,2}\xi_J) = 0. \qquad (7c)
\end{aligned}
$$

The above equations can be written in a matrix of $4 \times J$ order to calculate the eigenvalues and mode shapes:

$$[K(\omega)]\{C\} = 0. \qquad (8)$$

Theoretically, there seems no limit on calculating eigenvalues for any order mode from the above equations. In practice, however, it should be noted that when the frequency increases, the functions $\tanh(\lambda_{j+1,2})$ converge to unity, and the functions $\sinh(\lambda_{j+1,2})$ and $\cosh(\lambda_{j+1,2})$ become similar. This makes the last columns of the matrices in equations (6) and (8) converge to zero and also makes some of the other columns of the matrix in equation (8) tend to identical values. Therefore, at high frequencies the matrices become ill-conditioned, which makes numerical analysis for the eigensolutions difficult.

The first step towards overcoming this problem is to rebase the x-co-ordinate system in use to a local system where each plate element has its own co-ordinates based at its left edge (right edge and travelling in the leftwards direction for the first plate). Further, the hyperbolic terms in the shape function of equation (3) are replaced with exponential ones so that when the argument of the positive exponential term becomes large it can be suitable scaled, i.e., $C \sinh(\lambda_{i2}\xi) + D \cosh(\lambda_{i2}\xi)$ becomes $C \exp(-\lambda_{i2}\xi) + D \exp(\lambda_{i2}\xi)$ and when $\lambda_{i2}\xi$ is large $D \exp(\lambda_{i2}\xi)$ can be replaced with $D' \exp(-\lambda_{i2}(a_i/a - \xi))$. This reworking of the problem is then usually sufficient to ensure the matrix being dealt with is well behaved at all natural frequencies. Some problems do remain, however, when dealing with systems where nodal lines and joint lines coincide and these must be dealt with separately.

3. THE FINITE STRIP METHOD

The finite strip method may be considered as a special form of the FEM. The main difference may be said to be, taking a 2-D example, that the displacement function in the FSM combines a simple polynomial in the transverse direction and a continuously differentiable smooth series in the longitudinal direction, rather than the polynomials used in all directions in the FEM. Based on this special form of displacement function, the FSM

offers higher accuracy and smaller model sizes, since normally meshing in the longitudinal direction is unnecessary. For example, the general form of strip element displacement function for plate bending vibration can be represented by the product of a cubic Hermitian function in the x direction and a series of analytical vibration modes in the y direction as

$$W(\xi, \eta) = \sum_{n=1}^{r} f_n(\xi) Y_n(\eta) \tag{9}$$

where $Y_n(\eta)$ represents the nth term in a series of modes from the differential equation of a vibrating strip element (beam) obtained, *a priori*, (in the simply-supported case $Y_n(\eta) = \sin(n\pi\eta)$) which makes the $W(\xi, \eta)$ of type similar to equation (2) in the classical plate theory. However, the shape function $f_n()$ in the classical FSM normally takes a cubic Hermitian function represented in terms of the nodal coefficients, namely the transverse displacement h_{in} and rotation about the nodal line a_{in} corresponding to the nth term of $Y_n(\eta)$ as

$$f_n(\xi) = (1 - 3\xi^2 + 2\xi^3)h_{in} + l(\xi - 2\xi^2 + \xi^3)a_{in} + (3\xi^2 - 2\xi^3)h_{i+1,n} + l(-\xi^2 + \xi^3)a_{i+1,n}, \tag{10}$$

or in matrix form

$$f_n(\xi) = [C_1(\xi)C_2(\xi)C_3(\xi)C_4(\xi)]\{h\}_n, \tag{11}$$

where $\{h\}_n = \{h_{in}, a_{in}, h_{i+1,n}, a_{i+1,n}\}^{\mathrm{T}}$ is the nodal coefficient vector.

Since a cubic Hermitian function is chosen for the above shape function in the classical FSM, the solution accuracy depends upon the meshing size of the strip element model to a significant extent. In order to improve accuracy without increasing model size, the shape function should be exact and generated from the differential equation of a vibrating beam,

$$f''''(\xi) = \mu^4/l^4 f(\xi), \tag{12}$$

where l is the strip element length and $\mu^4 = \rho\omega^2 A l^4/EI$.

The general solution of equation (12) is a frequency-dependent function of a type similar to equation (3):

$$f(\xi, \eta) = A \sin(\mu\xi) + B \cos(\mu\xi) + C \sinh(\mu\xi) + D \cosh(\mu\xi). \tag{13}$$

By introducing the following boundary conditions of the element into equation (13),

$$\begin{aligned} f(\xi, \omega) &= h_1, \quad f'(\xi, \omega) = \theta_1 \quad \text{at} \quad \xi = 0, \\ f(\xi, \omega) &= h_2, \quad f'(\xi, \omega) = \theta_2 \quad \text{at} \quad \xi = l, \end{aligned} \tag{14}$$

the shape function can be written in terms of the nodal coefficients as

$$f(\xi, \omega) = S_1(\xi, \omega)h_1 + S_2(\xi, \omega)\theta_1 + S_3(\xi, \omega)h_2 + S_4(\xi, \omega)\theta_2. \tag{15}$$

Theoretically, such a shape function can be used to replace that in equation (10) for deriving the stiffness and mass matrices of the plate. However, since $f(\xi, \omega)$ is a function of ω, the stiffness and mass matrices obtained would be frequency dependent and cause some difficulty when solving the eigenproblem. In order to avoid this problem, the shape

function $f(\xi, \omega)$ can be assumed to be represented by a series in ascending powers of the frequency ω:

$$f(\xi, \omega) = \sum_{r=0}^{\infty} \omega^r [S(\xi)]_r \{h\}. \tag{16}$$

By substituting equation (16) into equation (12), one obtains

$$\sum_{r=0}^{\infty} \omega^r [S''''(\xi)]_r \{h\} - \omega^2 G \sum_{r=0}^{\infty} \omega^r [S(\xi)]_r \{h\} = 0, \tag{17}$$

where $G = \rho A/EI$.

By equating the coefficients of the same powers of ω in equation (17) to zero, the following equations can be obtained:

$$[S''''(\xi)]_0 = 0, \qquad [S''''(\xi)]_1 = 0, \qquad [S''''(\xi)_2 = G[S(\xi)]_0,$$
$$[S''''(\xi)_3 = G[S(\xi)]_1, \qquad \cdots, \qquad [S''''(\xi)_n = G[S(\xi)]_{n-2}, \qquad \cdots. \tag{18}$$

By solving equations (18), the functions $[S(\xi)]_r$ can be obtained and represented as

$$[S(\xi)]_0 = [(1 - 3\xi^2 + 2\xi^3)l(\xi - 2\xi^2 + \xi^3)(3\xi^2 - 2\xi^3)l(-\xi^2 + \xi^3)], \qquad [S(\xi)]_1 = 0,$$
$$[S(\xi)]_2 = \rho A l^4/2520EI[(66\xi^2 - 125\xi^3 + 105\xi^4 - 21\xi^6 + 6\xi^7)l(12\xi^2 - 22\xi^3 + 21\xi^5$$
$$- 14\xi^6 + 3\xi^7)(39\xi^2 - 54\xi^3 + 21\xi^6 - 6\xi^7)l(-9\xi^2 + 13\xi^3 - 7\xi^6 + 3\xi^7)],$$
$$[S(\xi)]_3 = 0, \qquad \cdots. \tag{19}$$

Substituting these functions into equation (16) yields a shape function of series type. Since the shape function is frequency dependent and satisfies the differential equation of a vibrating beam element, it is called a "dynamic" shape function.

Further, by substituting the "dynamic" shape function into equation (9), the displacement function can also be written in a series form as

$$W(\xi, \eta) = \sum_{n=1}^{N} ([S(\xi)]_0 Y_n(\eta) + \omega^2 [S(\xi)_2 Y_n(\eta) + \omega^4 [S(\xi)]_4 Y_n(\eta) + \cdots)\{h\}_n. \tag{20}$$

Using Hooke's Law and the relationship between displacement and strain gives $\sigma = [D]\varepsilon$, where

$$\varepsilon = \begin{Bmatrix} -\partial^2 W/\partial\xi^2 \\ -\partial^2 W/\partial\eta^2 \\ 2\partial^2/W/\partial\xi\partial\eta \end{Bmatrix} = \begin{Bmatrix} \sum_{n=1}^{N} (-[S''(\xi)]_0 Y_n(\eta) - \omega^2 [S''(\xi)]_2 Y_n(\eta) - \cdots)h_n \\ \sum_{n=1}^{N} (-[S(\xi)]_0 Y_n''(\eta) - \omega^2 [S(\xi)]_2 Y_n''(\eta) - \cdots)h_n \\ \sum_{n=1}^{N} (2[S'(\xi)]_0 Y_n'(\eta) + 2\omega^2 [S'(\xi)]2 Y_n'(\eta) + \cdots)h_n \end{Bmatrix}, \tag{21}$$

or

$$\varepsilon = ([B(\xi, \eta)]_0 + \omega^2[B(\xi, \eta)]_2 + \omega^4[B(\xi, \eta)]_4 + \cdots)\{h\}, \tag{22}$$

where

$$[B(\xi, \eta)]_i = \begin{Bmatrix} -\sum_{n=1}^{N} [S''(\xi)]_i Y_n(\eta) \\ -\sum_{n=1}^{N} [S(\xi)]_i Y_n''(\eta) \\ 2\sum_{n=1}^{N} [S'(\xi)]_i Y_n'(\eta) \end{Bmatrix}. \tag{23}$$

By applying the minimum potential energy principle, the strip element stiffness matrix can be obtained as

$$[K(\omega)] = \iint_t ([B(\xi, \eta)]_0 + \omega^2[B(\xi, \eta)]_2 + \cdots)^{\mathrm{T}}[D]([B(\xi, \eta)]_0 + \omega^2[B(\xi, \eta)]_2 + \cdots)\, \mathrm{d}\xi\, \mathrm{d}\eta. \tag{24}$$

This results in a strip element stiffness matrix of order 4N in a series matrix form:

$$[K(\omega)] = [K]_0 + \omega^2[K]_2 + \omega^4[K]_4 + \cdots. \tag{25}$$

In a similar way, the mass matrix of a consistent mass model can be also derived and written as

$$[M(\omega)] = [M]_0 + \omega^2[M]_2 + \omega^4[M]_4 + \cdots. \tag{26}$$

It is interesting to note that $[K_0]$ and $[M_0]$ appear to be identical with the $[K]$ and $[M]$ derived by the classical FSM, since the first term of the "dynamic" shape function is of the same type as the cubic Hermitian function used as the shape function in the classical FSM. This means that the $[K(\omega)]$ and $[M(\omega)]$ provide an extended and improved model for $[K]$ and $[M]$.

Since the discretization is carried out only in the x direction and the nodal coefficients are only related to the $f_n(x)$, the assembly of elements for the complete plate is carried out in one dimension in a similar manner to the FEM. The governing equation of the vibrating plate, ignoring the damping, can finally be obtained in the usual form as

$$([K]_0 + \omega^2[K]_2 + \cdots]) - \omega^2([M]_0 + \omega^2[M]_2 + \cdots)\{h\} = 0. \tag{27}$$

This equation is solved by first ignoring the higher order terms and using a standard QR algorithm, and then iteratively with each pair of additional terms in turn. There is normally no need to go beyond the terms in ω^2, however, as the series converges very rapidly.

4. NUMERICAL EXAMPLES

In order to demonstrate the application of the above methods, two simply supported steel plates with thickness changes as shown in Figures 1 and 2 are taken as examples.

In the first example, a thin square plate with $a = b = 1{\cdot}0$ m, $t_1 = 0{\cdot}001$ m and two

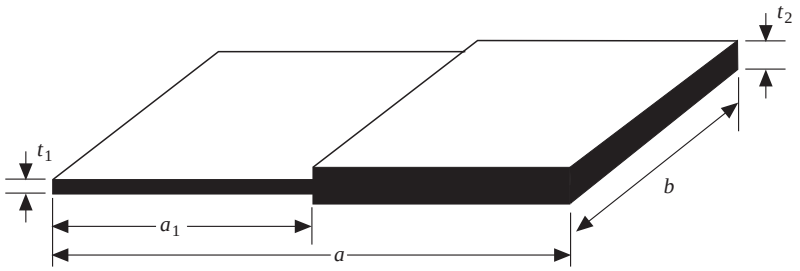

Figure 2. A simply supported stepped thickness plate.

stiffeners as shown in Figure 1 is chosen. In this example, three different thickness ratios of the stiffener to plate thickness $t_2/t_1 = 1{\cdot}0$, $1{\cdot}2$ and $1{\cdot}5$ are considered with joint lines located at $a_1 = 0{\cdot}3$, $a_2 = 0{\cdot}4$, $a_3 = 0{\cdot}6$ and $a_4 = 0{\cdot}7$ m. In modelling the plate by using classical analysis, the plate is divided into five parts which results in a set of 16 ordinary, linear simultaneous equations to solve. In the plate model when using FEM, 10×10 and 20×20 meshes are taken, respectively, for comparison with the other methods. This results in a FE model with matrix orders of 243 and 1083, respectively (four-noded rectangular elements with three degrees of freedom are used at each corner and fourth order Hermite polynomial shape functions with C1 continuity). In the FSM, only the first three terms of the $Y_i(y)$ series are taken to generate the strip element displacement function in the longitudinal y direction. In the transverse x direction, discretization is carried out by dividing the plate into 10 strip elements with four DOF in each element. This results in a 12×12 order matrix for each element model and 60×60 order for the whole plate model. The first eight natural frequencies obtained by the above three methods are compared in Table 1. Here, the classical analysis takes around two seconds to find the eight frequencies for a single plate geometry when using a Sun Ultra 2 model 140, the FSM slightly less than one s for either static or dynamic formulations and the FEM about 50 s for the 10×10 mesh and 3100 s for the 20×20 mesh.

Consider first the results from the 10×10 mesh case when using the FEM and compare these with the results of the classical method; see Table 1. It is seen that the accuracy of solutions drops as the order of the modes increases, as expected. To take the uniform thickness case as an example, the frequency errors of mode 1 and mode 8 are 0·7% and 7·2%, respectively. This shows that the solution accuracy of the FEM is heavily dependent upon the element size. By refining the mesh to 20×20, the accuracy of all solutions is improved significantly, with reduced frequency errors of 0·2% for mode 1 and 1·9% for mode 8, respectively. However, the cost of computing time has increased significantly. Secondly, by using the FSM, which generates a much smaller model size and therefore is more efficient than the FEM, it is seen that virtually perfect solution accuracy is obtained for all modes and all three thickness ratios. Lastly, it is noted that the FSM method with 10 strip elements is sufficient to generate accurate solutions with or without the "dynamic" element formulation in this case.

In the second example, a square plate of $a = b = 1{\cdot}0$ m and $t_1 = 0{\cdot}001$ m, as per example 1, but with a stepped thickness as shown in Figure 2 is considered. In this example, three different thickness ratios of $t_2/t_1 = 1{\cdot}0$, $1{\cdot}25$ and $2{\cdot}0$ are taken with the joint line location at $a_1 = 0{\cdot}5$ m. In the classical method this time the plate is divided into two parts, resulting in a set of eight equations. In the FEM, 10×10 and 20×20 meshes are again taken. In the FSM, however, the plate is divided into only four strip elements. This results in a 24×24 order matrix for the whole plate model. Obviously, the model size of the FSM

TABLE 1

Comparison of natural frequencies (rad/s) for example 1 (*bracketed terms are for* FEM *with a* 20 × 20 *mesh or the "dynamic"* FSM)

Mode no.	$t_2/t_1 = 1{\cdot}0$			$t_2/t_1 = 1{\cdot}2$			$t_2t_1 = 1{\cdot}5$		
	CM	FEM	FSM	CM	FEM	FSM	CM	FEM	FSM
1	30·67	30·88	30·67	31·74	31·95	31·74	33·17	33·39	33·17
	–	(30·73)	(30·67)	–	(31·79)	(31·74)	–	(33·23)	(33·17)
2	76·68	77·66	76·68	79·30	80·69	79·30	81·69	83·26	81·70
	–	(76·94)	(76·68)	–	(79·70)	(79·29)	–	(82·11)	(81·69)
3	76·68	79·01	76·69	80·60	82·64	80·60	87·64	89·78	87·68
	–	(77·27)	(76·68)	–	(81·07)	(80·60)	–	(88·20)	(87·67)
4	122·7	125·6	122·7	127·3	130·3	127·3	134·2	137·4	134·2
	–	(123·5)	(122·7)	–	(128·2)	(127·3)	–	(135·1)	(134·2)
5	153·4	160·9	153·4	156·4	164·2	156·4	161·5	169·3	161·6
	–	(155·3)	(153·4)	–	(158·3)	(156·3)	–	(163·5)	(161·5)
6	153·4	161·4	153·4	162·5	170·9	162·5	179·0	188·8	179·1
	–	(155·4)	(153·4)	–	(164·6)	(162·4)	–	(181·6)	(179·0)
7	199·4	202·7	199·4	207·1	211·0	207·2	221·1	224·6	221·2
	–	(200·4)	(199·3)	–	(208·5)	(207·0)	–	(222·7)	(221·0)
8	199·4	213·7	199·4	207·8	222·5	207·8	222·0	237·9	222·0
	–	(203·2)	(199·4)	–	(211·5)	(207·7)	–	(226·0)	(221·8)

in this example is significantly reduced compared with example 1 and is much smaller than that for the FEM.

First, from comparison of the classical method and the FEM results for this example (see Table 2), comments may be made similar to those about Table 1 for the first example: i.e., errors increase with mode number and thickness change and decrease with increasing mesh density. Secondly, comparing the results in Table 2 for the classical method and the

TABLE 2

Comparison of natural frequencies (rad/s) for example 2 (*bracketed terms are for* FEM *with a* 20 × 20 *mesh or the "dynamic"* FSM, *note also that the classical method results differ from those of* Chopra *due to the incorrect boundary conditions used in that work*; see text)

Mode no.	$t_2/t_1 = 1{\cdot}0$			$t_2/t_1 = 1{\cdot}25$			$t_2t_1 = 2{\cdot}0$		
	CM	FEM	FSM	CM	FEM	FSM	CM	FEM	FSM
1	30·67	30·88	30·68	34·23	34·47	34·50	44·50	44·85	45·22
	–	(30·73)	(30·66)	–	(34·29)	(34·48)	–	(44·59)	(45·18)
2	76·68	77·66	76·69	85·69	87·07	86·19	109·1	111·2	110·9
	–	(76·94)	(76·64)	–	(86·12)	(85·83)	–	(109·8)	(110·2)
3	76·68	79·01	76·88	86·33	88·70	88·55	110·2	113·3	113·3
	–	(77·27)	(76·63)	–	(86·85)	(88·11)	–	(110·9)	(112·6)
4	122·7	125·6	122·8	137·7	140·9	140·9	172·6	176·9	178·2
	–	(123·5)	(122·8)	–	(138·6)	(140·8)	–	(173·8)	(178·1)
5	153·4	160·9	153·4	169·3	177·8	169·8	197·3	206·7	198·0
	–	(155·3)	(153·3)	–	(171·5)	(169·7)	–	(199·8)	(197·7)
6	153·4	161·4	155·7	169·8	178·5	177·9	211·4	221·5	237·6
	–	(155·4)	(153·8)	–	(171·9)	(173·6)	–	(214·0)	(226·4)
7	199·4	202·7	199·5	222·1	227·1	229·2	287·2	296·2	299·8
	–	(200·4)	(195·1)	–	(224·1)	(222·5)	–	(290·4)	(285·8)
8	199·4	213·7	201·3	224·6	239·4	231·9	293·2	310·6	322·3
	–	(203·2)	(197·3)	–	(228·1)	(228·3)	–	(297·6)	(292·7)

FSM, it is noted that the effect of model size reduction on the accuracy for the uniform thickness case is less than 1% at worst. However, errors in the results for the stepped thickness cases when using the classical FSM are now quite significant due to the reduction in the number of elements and consequent model size. The reason for this is mainly because, as described in section 3, the approximation of the cubic Hermitian function used as the shape function for representing the strip element deflection in the transverse direction becomes poor when the element size increases in that direction. Therefore, improvement of the shape function by using the dynamic FSM should be expected to increase the solution accuracy, as seen in Table 2. By applying the dynamic FSM to the stepped thickness cases, the results at all frequencies have been improved, although this improvement varies with the number of half wavelengths exhibited by the modes in the strip direction, as might be expected. It is clear that the "dynamic" finite strip method is dramatically more efficient than traditional finite elements in this case.

5. CONCLUSIONS

The free vibration analysis of a stepped, simply supported thin plate has been investigated by applying classical, finite strip and finite element methods. Effort has been made to deal with and overcome the difficulties occurring when calculating high order modes using classical methods. The approach adopted eliminates the upper frequency range limit associated with the numerical difficulties inherent in a simplistic application of classical methods to such problems. The classical finite strip method has also been improved by developing a dynamic shape function in series form to replace the "static" cubic Hermitian function. Because of the shape function improvement, the dependence of the solution accuracy upon the strip element size can be largely reduced. Therefore, solution accuracy can be improved without increasing model size. This allows reduced computing effort and improves analysis efficiency. When compared with the traditional FEM, this advantage is even more significant.

ACKNOWLEDGMENT

This work has been supported by the EPSRC under grant no. GR/J06856 which is gratefully acknowledged.

REFERENCES

1. K. M. Liew and K. Y. Lam 1990 *Journal of Sound and Vibration* **139**, 241–252. Application of two-dimensional orthogonal plate functions to flexural vibrations of skew plates.
2. K. M. Liew, K. Y. Lam and S. T. Chow 1990 *Computers and Structures* **34**, 79–85. Free vibration analysis of rectangular plates using orthogonal plate function.
3. Y. K. Cheung 1976 *Finite Strip Method in Structural Analysis*. Oxford: Pergamon.
4. J. S. Przemieniecki 1968 *Theory of Matrix Structural Analysis*. New York: Dover Publications.
5. X. J. Chen and L. C. Zhao 1982 *Dynamic Finite Element Method in Bending Plate Vibration Analysis*, *Vibration and Shock* (*in Chinese*).
6. N. Mukherjee and T. Chattopadhyay 1994 *Computers & Structures* **52**, 259–264. Improved free vibration of stiffened plate by dynamic element method.
7. Y. K. Cheung and J. Kong 1995 *Journal of Sound and Vibration* **181**, 341–353. The application of a new finite strip to the free vibration of rectangular plates of varying complexity.
8. I. Chopra 1974 *International Journal of Mechanical Science* **16**, 337–344. Vibration of stepped thickness plates.

APPENDIX: NOTATION

a, b	dimensions of plate, see Figures 1 and 2
a_i, t_i	step length and thickness of the ith part of the plate, see Figure 1
A, l	cross-sectional area and length of a beam element
$A_{in}, B_{in}, C_{in}, D_{in}$	coefficients in the nth shape function of the ith part of a vibrating plate
D_i	plate rigidity corresponding to t_i, $Et_i^3/12(1-\nu^2)$
E	Young's modulus
I	moment of inertia of cross-sectional area
J	number of joints in the plate
n	number of half sine waves in y direction
$W_i(x, y)$	shape function of the ith part of the plate
x, y	rectangular coordinates
ξ, η	non-dimensional co-ordinates x/a and y/b, respectively
ρ, ν	material density and Poisson's ratio
k_i^4	$\rho\omega^2 t_i/D_i$
ω	radian frequency of oscillation
$\lambda_{i1}, \lambda_{i2}$	$a\sqrt{k_i^2-\alpha^2}, a\sqrt{k_i^2+\alpha^2}$
α	$n\pi/b$
$\mathbf{V}^2$	Laplacian in rectangular co-ordinates.